

# RSC Advances



This is an *Accepted Manuscript*, which has been through the Royal Society of Chemistry peer review process and has been accepted for publication.

*Accepted Manuscripts* are published online shortly after acceptance, before technical editing, formatting and proof reading. Using this free service, authors can make their results available to the community, in citable form, before we publish the edited article. This *Accepted Manuscript* will be replaced by the edited, formatted and paginated article as soon as this is available.

You can find more information about *Accepted Manuscripts* in the [Information for Authors](#).

Please note that technical editing may introduce minor changes to the text and/or graphics, which may alter content. The journal's standard [Terms & Conditions](#) and the [Ethical guidelines](#) still apply. In no event shall the Royal Society of Chemistry be held responsible for any errors or omissions in this *Accepted Manuscript* or any consequences arising from the use of any information it contains.

## Silicalite-1/glass fibre substrates for enhancing the photocatalytic activity of TiO<sub>2</sub>

Cite this: DOI: 10.1039/x0xx00000x

F.T. Ozkan, R. Quesada-Cabrera and I.P. Parkin\*

Received ooth,  
Accepted ooth

DOI: 10.1039/x0xx00000x

www.rsc.org/

Silicalite-1 (S1) coatings were prepared on silica wool substrates by hydrothermal synthesis and subsequently immersed into a Ti-containing sol at a steady rate of 30 cm min<sup>-1</sup>. The material was annealed in a furnace at 90 °C for 2 h and 550 °C for 2 h to create a silica fibre core surrounded by concentric layers of silicalite-1 and TiO<sub>2</sub>. The resulting samples were characterised by X-ray diffraction (XRD), Raman spectroscopy, scanning electron microscopy (SEM), X-ray photoelectron spectroscopy (XPS) and Brunauer-Emmett-Teller (BET) surface area measurement. The photocatalytic activity of the samples was evaluated using the intelligent ink test and during degradation of stearic acid under UVA light ( $\lambda = 365$  nm). The new coated-fibres were shown to be substantially better photocatalysts than comparable TiO<sub>2</sub> coatings on plain glass fibres. The TiO<sub>2</sub>/S1/glass fibres have potential use in air/water cleaning applications.

### Introduction

The immobilisation of photocatalysts has been identified as key factor in photoreactor design for environmental applications.<sup>1</sup> The process of filtration and resuspension of powders is a major disadvantage in the efficient performance of photoreactors. Removing photocatalysts in powder form from the solution can be very difficult and the particles tend to aggregate during the cycle process, reducing considerably their activity. As reviewed recently,<sup>1</sup> various strategies have been followed in the structural design of filters involving the use of non-woven fabric, ceramic foams, porous materials, etc. These supports are devised to offer high surface-to-volume ratios and –in the case of those composed by fibres, they can be conveniently light, flexible and cost-effective. Woven glass meshes and glass wool have been widely used as substrates for titanium dioxide (TiO<sub>2</sub>)-based materials in photoreactors for water and air cleaning applications.<sup>2-10</sup> The deposition of TiO<sub>2</sub> on glass fibres is beneficial in terms of active surface area exposed and interfacial charge carrier transfer rate, which are key features in the efficiency of photocatalytic systems. Unfortunately, the immobilisation of TiO<sub>2</sub> on plain glass fibres reduces the

specific surface area of the photocatalyst relative to the powder form.

An interesting and simple approach to promote roughness on glass fibres is the interpolation of high-surface area coating materials previous to the deposition of TiO<sub>2</sub>. Conveniently, many zeolites can be grown as continuous films on fibrous materials.<sup>11-15</sup> Zeolites are crystalline microporous materials that have been used in many applications and chemical processes in industry, including adsorption, ion-exchange, catalysis, etc. Some zeolites have been effectively combined with TiO<sub>2</sub>, taking advantage of their active participation in electron-transfer processes, in order to enhance photocatalytic activity.<sup>16-18</sup> These TiO<sub>2</sub>/zeolite systems have been made in powder form<sup>16, 19, 20</sup> or as sheets by a papermaking technique.<sup>21, 22</sup> However, the latter forms still lead to the same technical disadvantages observed in the use of photocatalysts in powder form, such as undesirable particle agglomeration and the need of further separation processes in the slurry material after the photocatalytic reaction.

Silicalite-1 (S1) is a well-known MFI-type zeolite and a model system in studies of hydrothermal crystal growth.<sup>23</sup> This zeolite

has been successfully used in combination of TiO<sub>2</sub> in the treatment of volatile organic compounds.<sup>24</sup> In that work, the S1 zeolite was grown directly on stainless steel sheets as part of a membrane-catalyst for the degradation of trichloroethylene. Here, highly photoactive systems were prepared by direct hydrothermal deposition of a thin layer of silicalite-1 on both glass fibres (silica wool) and glass slides, followed by the deposition of TiO<sub>2</sub> as synthesised using a sol-gel method. The process is described in the schematic diagram presented in Figure 1. The silica wool is commercially available and consists of long amorphous silica fibres with diameter of *ca.* 5–20 μm.<sup>13</sup> After the incorporation of the zeolite layer, a significant change in surface area resulted in a drastic enhancement of photocatalytic activity, as evaluated during the degradation of stearic acid and the reduction of resazurin dye.

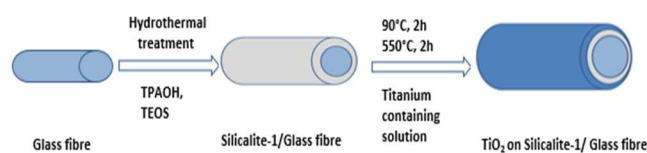


Figure 1 – Schematic diagram illustrating the deposition steps described in this work. A first layer of silicalite-1 zeolite is deposited on glass fibres (silica wool) *in situ* during hydrothermal synthesis and then calcined in two steps at 90 °C (2 h) and 550 °C (2 h). A second layer was then dip-coated from sol-gel solution and finally annealed at 550 °C.

## Results and discussion

**Synthesis and characterisation of TiO<sub>2</sub>/silicalite-1/glass fibre materials.** The silicalite-1 zeolite was synthesised via one- and two-step hydrothermal methods adapted from the literature.<sup>13</sup> The specific details of the synthesis are given in the Experimental section. Tetrapropylammonium hydroxide (TPAOH) and tetraethyl orthosilicate (TEOS) were used as template agent and silicate sources, respectively. The reaction conditions are given in Table 1. The glass fibres were included in the hydrothermal treatment for the deposition of the resulting silicalite-1 material.

The synthesis of TiO<sub>2</sub> was carried out following a sol-gel method based on the hydrolysis of a titanium precursor and its subsequent polymerization into a Ti-O-Ti network.<sup>25</sup> The silicalite-1/glass fibre material was dip-coated into the sol-gel (withdrawal rate of 30 cm min<sup>-1</sup>) so that a thin layer of the titania precursor is deposited on the substrates surface and the gelation of the sol is substantially accelerated. During dip-coating, aggregation, gelation and drying occur in seconds to minutes comparing to bulk sol-gel systems.<sup>26, 27</sup> The deposition of TiO<sub>2</sub> on plain glass wool was also carried out by dip-coating and used as reference material. The films are chemically bonded to the surface of the glass fibres via a condensation reaction of the titanium alkoxide/hydroxide with surface bound hydroxyl groups.<sup>25</sup> Annealing of the samples at 550 °C ensured the removal of any remaining solvents, alkoxy and hydroxyl

groups and seemingly improved the packing of the Ti-O-Ti polymer system into a crystalline anatase network.

Table 1 – Synthesis conditions of the silicalite-1 material prepared by one- and two-step hydrothermal synthesis. The gel types used in the synthesis refer to: (A) TPAOH (2.0 g), TEOS (10.4 g) and water (15.1 ml) and (B) TPAOH (1.2 g), TEOS (10.4 g) and water (15.1 ml). The BET surface areas indicated were obtained from the annealed samples after deposition of the TiO<sub>2</sub> layer. The BET results for plain fibres and direct TiO<sub>2</sub>-coated fibres were 5 and 10 m<sup>2</sup> g<sup>-1</sup>, respectively.

Samples	Gel	Hydrothermal synthesis conditions				BET (m <sup>2</sup> g <sup>-1</sup> )
		1 step		2 step		
		T (°C)	t (h)	T (°C)	t (h)	
1A	A	170	6	–	–	73
2A	A	130	4	150	3	57
3A	A	130	3	170	2	58
4A	A	130	22	–	–	109
1B	B	170	6	–	–	58
2B	B	130	4	150	3	46
3B	B	130	3	170	2	44
4B	B	130	22	–	–	51

A series of TiO<sub>2</sub>/silicalite-1/glass fibre samples were prepared, as shown in Table 1. The samples are denoted as (1–4)A and (5–8)B according to the hydrothermal conditions used for the synthesis of the silicalite-1/glass fibre materials (Table 1). Correspondingly, the TiO<sub>2</sub>/silicalite-1/glass fibre samples are denoted as TiO<sub>2</sub>/1A, TiO<sub>2</sub>/2A, etc.

The chemical composition of the glass fibre surface treated with silicalite-1 and TiO<sub>2</sub> was characterized by XPS analysis. Figure 2(a) shows the XPS survey spectra of the as-deposited samples. In the quantitative analysis of the films, carbon, oxygen, titanium and silicon were detected. The limitations used for fitting the Ti 2p XPS spectra refer to the relation between integral intensities of these doublet components  $2 \times 2p_{1/2} = 2p_{3/2}$  (Figure 2(b)). The two doublet separation was 5.76 eV.<sup>28</sup> The peaks were assigned to Ti 2p<sub>1/2</sub> and 2p<sub>3/2</sub>, located at binding energies of 464.3 and 458.6 eV respectively.<sup>29, 30</sup> Si 2p peaks were found at 103.5 eV, coming from glass fibre and/or silicalite-1 (Figure 2(a)).<sup>31</sup> The XPS analysis of the O 1s peak (Figure 2(c)) showed two different environments for oxygen, namely Si-O-Si labelled at 532.9 eV and either Ti-O-Ti in the TiO<sub>2</sub> lattice or H-O bonds of the surface hydroxyl groups at 530.0 eV.<sup>32, 33</sup> XPS showed only the expected elements Ti, Si, O with some residual carbon.

The structural properties of the as-deposited TiO<sub>2</sub>/silicalite-1/glass fibre materials were studied by XRD and Raman spectroscopy (Figure 3). Although the amorphous nature of the glass fibres dominated the XRD patterns (broad feature at

$5^\circ/2\theta$ ), sharp reflection peaks confirmed the presence of both anatase  $\text{TiO}_2$  and silicalite-1 compounds on the glass wool.<sup>13</sup> The intense reflections in the range of  $3\text{--}4^\circ/2\theta$  and  $10\text{--}11^\circ/2\theta$  are due to the silicalite-1 MFI structure.<sup>13</sup> Most of the rest are due to  $\text{TiO}_2$  anatase phase, with the dominant characteristic (101) peak at  $11.5^\circ/2\theta$  (Figure 3). There was no evidence of the rutile form in the XRD patterns. Further structural analysis was attempted using Raman spectroscopy. The characteristic bands of anatase  $\text{TiO}_2$  were clearly observed at 144 ( $E_g$ ), 197 ( $E_g$ ), 400 ( $B_{1g}$ ), 525 ( $A_{1g} + B_{1g}$ ) and 634 ( $E_g$ )  $\text{cm}^{-1}$ .<sup>34</sup> However, the Raman spectrum of silicalite-1 is typically weak and a strong fluorescence hindered the assignment of the zeolite bands. No evidence of rutile or any other phases were identified.

SEM was used to study the morphology of the uncoated and coated glass fibre surfaces with silicalite-1 and  $\text{TiO}_2$  coatings, as shown in Figure 4. The SEM analysis revealed that the direct deposition of  $\text{TiO}_2$  on glass wool was highly heterogeneous and partial delamination was clearly observed across the fibre (Figure 4(b)). In general, the microstructural properties of the silicalite-1 layer were similar in all the samples synthesised in this work, consisting of rectangular plates.<sup>35, 36</sup> However, the coating of the fibres in the latter case was strongly depended on the synthesis conditions. As a case study, Figure 4(c) and 4(d) show typical zeolite-coated fibres in samples 2A and 3B, respectively. It can be observed that, despite the higher concentration of precursor template agent (TPAOH) and longer annealing times involved in the synthesis of sample 2A (Table 1), sample 3B showed rougher coatings and larger zeolite particles, likely due to the high temperature conditions ( $170^\circ\text{C}$ ) used during the second hydrothermal treatment compared to sample 2A ( $150^\circ\text{C}$ ).

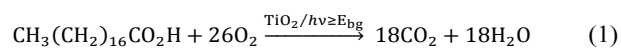
The influence of annealing time on the zeolite coating quality was further studied by comparison of samples 2A and 4A (Figure 5(a) and 5(b), respectively). Sample 2A was synthesised following a two-step hydrothermal process (Table 1), with an initial annealing period of 4 h at  $130^\circ\text{C}$  and a second one of 3 h at  $150^\circ\text{C}$ , whilst sample 4A was produced after a single step of 22 h at  $130^\circ\text{C}$ . It was interesting to note that, whereas the morphology of both materials was apparently similar, the corresponding surface areas were significantly different, according to BET surface analysis. The BET area of plain glass fibres was  $5\text{ m}^2\text{ g}^{-1}$  and it increased to ca.  $10\text{ m}^2\text{ g}^{-1}$  after deposition of  $\text{TiO}_2$ . In general, it was observed that the zeolite samples prepared from gel A had a higher surface area than those produced from gel B under the same conditions. The BET areas of the  $\text{TiO}_2/\text{S1}/\text{fibre}$  systems are shown in Table 1. A general decrease in surface area was observed after the  $\text{TiO}_2$  coating, which is likely due to the obstruction of zeolite pores in the dip-coating process. Sample 4A showed the highest surface area and underwent the longest hydrothermal treatment,  $130^\circ\text{C}$  over 22 h, during the silicalite-1 preparation process using high TPAOH concentration (Table 1). It was interesting to note that sample 4B, synthesised under similar temperature conditions as those used for sample 4A but roughly half the

amount of TPAOH, showed substantially reduced surface area, despite the apparently similar morphology of both materials (Figure 5(c) and 5(d)).

The  $\text{TiO}_2$  film thickness was measured by using cross-section SEM images of the samples. The  $\text{TiO}_2$  layer was clearly observed in unevenly coated fibres (Figure 6(a)). The thickness ranged between 350–1300 nm and the average was  $\sim 650$  nm. The cracks observed in the  $\text{TiO}_2$  coating (Figure 6(b)) occurred during annealing, as due to thermal expansion coefficient differences between the  $\text{TiO}_2$  layer and the substrate.<sup>37</sup>

**Photocatalytic activity of  $\text{TiO}_2/\text{silicalite-1}/\text{glass}$  systems.** The photocatalytic activity of the  $\text{TiO}_2/\text{S1}/\text{glass}$  systems was initially screened using the intelligent ink test under UVA illumination ( $1\text{ mW cm}^{-2}$ ).<sup>38</sup> The details of this test are given in the experimental section. It is based on the irreversible photoreduction of resazurin dye molecule to resorufin, which involves a colour change from blue to pink, in the presence of a sacrificial electron donor (in this case, glycerol).<sup>38</sup> The results of the ink test are shown in Figure 7. The amount of  $\text{TiO}_2$  deposited on the glass fibres and also the amount of wool used in the photocatalytic testing was difficult to control. Therefore, the different  $\text{TiO}_2$  and S1 layers were deposited on glass slides for the test, allowing fair comparison between the materials and highlight the effect of using the S1 substrate in the system. As expected, the colour of the ink changed from blue to pink during irradiation of all  $\text{TiO}_2$ -containing samples (Figure 7). Further irradiation degraded the ink system and the colour disappeared. No photo-reduction of the resazurin dye was observed for glass wool or silicalite-1/glass fibre materials in the absence of  $\text{TiO}_2$ . It was interesting to note that, while the reduction of the ink is only noticeable after  $\sim 1$  h irradiation ( $1\text{ mW cm}^{-2}$ ) on  $\text{TiO}_2$  deposited on plain glass, the reaction readily occurred within 15 min in the case of the  $\text{TiO}_2/\text{S1}/\text{glass}$  slide. At the same time, clear signs of reduction were noticed for the  $\text{TiO}_2/\text{S1}/\text{fibre}$  system within the initial minutes of irradiation (Figure 7).

Further photocatalytic testing was carried out during the photo-induced mineralisation of a model organic pollutant, octadecanoic (stearic) acid. The degradation reaction is expressed by Equation (1) and typically monitored using infrared spectroscopy.<sup>39</sup>



The photocatalytic reaction rate is estimated from integrated areas of typical C–H bands of the acid at 2958, 2923 and 2853  $\text{cm}^{-1}$ . In the calculation of the reaction rate, linear regression is estimated from the initial zero-order kinetics reaction steps (30–40%). An estimation of the number of molecules of stearic acid degraded on the film can be obtained using a conversion factor ( $1\text{ cm}^{-1} \equiv 9.7 \times 10^{+15}$  molecules) reported in the literature.<sup>39</sup> The photocatalytic activity of the catalyst is widely

expressed in terms of formal quantum efficiency (FQE), defined as the number of acid molecules degraded per incident photon.

Figure 8(a) shows the curves of integrated areas during UVA irradiation ( $3.7 \text{ mW cm}^{-2}$ ) over 20 h. As it can be seen, the acid is very stable under UVA light over the test period. As expected, the results confirmed the photocatalytic behaviour of the films observed in the preliminary ink testing. Complete mineralisation of the stearic acid was only observed on the  $\text{TiO}_2/\text{S1}/\text{glass}$  system over the course of the experiment. It was interesting to note that the silicalite-1 material deposited on plain glass (no  $\text{TiO}_2$ ) also showed some photocatalytic activity beyond instrumental error (Figure 8(a)). This is in contrast with former studies involving silicalite-1, where no photocatalytic activity was observed in the degradation of trichloroethylene.<sup>24</sup> The corresponding formal quantum efficiencies (FQE) estimated are shown in Figure 8(b). The FQE of the  $\text{TiO}_2/\text{S1}/\text{glass}$  system was 6 times that of the  $\text{TiO}_2$  layer deposited on glass. The enhanced activity was attributed to the roughening effect of the zeolite layer rather than to the zeolite intrinsic surface area, since it is unlikely that the underpinning nanoporosity of the zeolite will affect the photocatalysis performance of the system.

## Conclusions

A range of  $\text{TiO}_2/\text{silicalite-1}$  (S1)/glass fibre materials were hydrothermally prepared under different synthesis conditions (temperature, annealing time and precursor concentration), as indicated in **Table 1**, and their photocatalytic activity correlated with surface roughness. The deposition of the S1 zeolite on glass fibres (silica wool) was carried out in situ during the hydrothermal process and the  $\text{TiO}_2$  layer was dip-coated from a sol-gel mixture and calcined at  $90^\circ\text{C}$  for 2 h and  $550^\circ\text{C}$  for 2 h. The photocatalytic activity of the films was first screened during photoreduction of the resazurin dye system ("intelligent ink") under UVA irradiation and also evaluated during mineralisation of stearic acid. The photocatalytic activity of the  $\text{TiO}_2/\text{S1}/\text{glass}$  film was 6 times higher than that of the pure anatase  $\text{TiO}_2$  layer on glass, as expected from the corresponding increase in surface area.

This efficient, cost-effective photocatalytic system is perceived as a promising material for environmental applications, in particular as a filter for air cleaning photoreactors.

## Experimental

All chemicals used in this work were purchased from *Sigma-Aldrich*: glass (silica) wool, TPAOH (Tetrapropylammonium hydroxide) 1M in  $\text{H}_2\text{O}$ , TEOS (Tetraethyl orthosilicate),  $\geq 99.0\%$ ; acetylaceton, 99%; isopropanol, 99.5%; titanium(IV) n-butoxide, 97%; butan-1-ol, 99.8%; acetonitrile, 99%; resazurin, 92%; glycerol, 99.5%; Hydroxy ethyl cellulose (average  $M_n = 90,000$ ); stearic acid,  $\geq 95\%$ .

## Synthesis of the $\text{TiO}_2/\text{silicalite-1}/\text{fibre}$ materials

In the synthesis of silicalite-1, 10 mmol of TPAOH (tetrapropylammonium hydroxide) were mixed with 50 mmol of TEOS (tetraethyl orthosilicate) in 15 ml of distilled water under strong stirring conditions for 30 min. The mixture was then heated in teflon-lined stainless steel autoclave at different temperatures and time periods, as indicated in Table 1. For the synthesis of  $\text{TiO}_2$ , 50 mmol of titanium n-butoxide were added to a solution of acetylaceton (25 mmol) in 32 ml of butan-1-ol (350 mmol) under strong stirring conditions during 1 hour. The solution turned from clear, colourless to pale straw yellow without any precipitation. 3.6 ml of an aqueous solution of isopropanol (150 mmol) were mixed with the titanium n-butoxide solution. The sol remained clear but deepened in yellow colour after stirring for an hour, which was followed by the addition of acetonitrile (40 mmol) and stirred for another hour. The sol-gel was finally left overnight. The material was first dried at  $90^\circ\text{C}$  for 2 hours and then calcined at  $550^\circ\text{C}$  for another 2 hours, and was allowed to cool down to room temperature overnight.

## Characterization techniques

X-ray diffraction patterns were carried out using a Stoe diffractometer with monochromated  $\text{Mo K}\alpha 1$  radiation ( $\lambda = 0.7093 \text{ \AA}$ ) in transmission mode over the angle range  $2-40^\circ/2\theta$ . In the XRD analysis, the samples were ground gently and sieved in order to isolate the coating materials from the amorphous glass fibres. Raman spectroscopy was performed using a Renishaw Raman system 1000 equipped with a helium-neon laser ( $\lambda = 514.5 \text{ nm}$ ). Scanning electron microscopy (SEM) analysis was achieved on gold-sputtered samples using a Jeol JSM-6301F. The SEM images were obtained using SEMAfore software. A pinch of the samples were taken and coated with a film layer of gold to avoid charging. An X-ray photoelectron spectroscopy (XPS) was carried out using a Thermo Scientific K-Alpha instrument with monochromatic  $\text{Al-K}\alpha$  source for the analysis of chemical composition and oxidation states of the samples. High resolution scans were obtained for Ti (2p), C(1s), O(1s) and Si(2p). C 1s was recorded for calibration of the spectrometer.<sup>40</sup> The peaks were modelled using CASAXPS software with binding energies calibrated to adventitious carbon (285 eV). Brunauer-Emmett-Teller (BET) surface area measurements were carried out using a Micromeritics ASAP 2420 Accelerated Surface Area and Porosimetry System. Each sample was weighed to *ca.* 0.2 g and then degassed at  $150^\circ\text{C}$  in  $\text{N}_2$  for 12 hours before analysis.

## Photocatalytic tests

Resazurin ink was prepared following a procedure from the literature.<sup>39</sup> The ink consisted of 0.3 g of hydroxy ethyl cellulose (HEC) polymer, 3 g of glycerol and 0.04 g of resazurin dye in an aqueous solution that was aged for 24 hours at  $3-5^\circ\text{C}$ . An aerosol spray-gun was filled with this indicator ink and used to coat the specified surface area of the samples evenly. The photocatalytic reduction of resazurin was observed

by digital photographic methods. For the stearic acid test, a thin layer of the acid was deposited by dip-coating the films into a 0.05 M chloroform solution. The films were irradiated under UVA illumination ( $\lambda = 365$  nm) using BLB lamps (*Vilber-Lourmat*,  $2 \times 8$  W, 1 and 3.7 mW cm<sup>-2</sup> for the ink and stearic acid tests, respectively). The mineralisation of stearic acid bands at 2700–3000 cm<sup>-1</sup> was monitored using a Perkin-Elmer RX-I Fourier Transform Infrared Spectrometer.

## Acknowledgements

Kevin Reeves, Steven Firth and Martin Vickers are thanked for assistance with SEM, Raman spectroscopy and XRD instruments. FTO is funded by The Turkish Ministry of National Education.

## Notes

Materials Chemistry Research Centre, Department of Chemistry, University College London, 20 Gordon Street, London WC1H 0AJ, UK. E-mail: [i.p.parkin@ucl.ac.uk](mailto:i.p.parkin@ucl.ac.uk)

## References

1. T. Ochiai and A. Fujishima, *Journal of Photochemistry and photobiology C: Photochemistry reviews*, 2012, **13**, 247-262.
2. X. Zhang, Y. Li, Z. Lin and S. Zhang, in *Advanced Materials, Pts 1-4*, eds. Z. Cao, X. Q. Cao, L. Sun and Y. H. He, Editon edn., 2011, **239-242**, pp. 571-574.
3. H. G. Yu, S. C. Lee, J. G. Yu and C. H. Ao, *Journal of Molecular Catalysis a-Chemical*, 2006, **246**, 206-211.
4. H. Yu, S. C. Lee, C. H. Ao and J. Yu, *Journal of Crystal Growth*, 2005, **280**, 612-619.
5. C. H. Ao, S. C. Lee and J. C. Yu, *Journal of Photochemistry and Photobiology a-Chemistry*, 2003, **156**, 171-177.
6. V. Brezova, A. Blazkova, L. Karpinsky, J. Groskova, B. Havlinova, V. Jorik and M. Ceppan, *Journal of Photochemistry and Photobiology a-Chemistry*, 1997, **109**, 177-183.
7. C.-N. Kuo, H.-F. Chen, J.-N. Lin and B.-Z. Wan, *Catalysis Today*, 2007, **122**, 270-276.
8. W. Liu, L. Zhang, L.-X. Cao, G. Su and Y.-G. Wang, *Journal of Alloys and Compounds*, 2011, **509**, 3419-3424.
9. J. Palau, M. Colomer, J. M. Penya-Roja and V. Martinez-Soria, *Industrial & Engineering Chemistry Research*, 2012, **51**, 5986-5994.
10. D. Robert, A. Piscopo, O. Heintz and J. V. Weber, *Catalysis Today*, 1999, **54**, 291-296.
11. A. E. Comyns, *Applied Organometallic Chemistry*, 1999, **13**, 209-210.
12. R. M. Barrer, *Hydrothermal chemistry of zeolites*, Academic Press, London; New York, 1982.
13. O. Larlus, V. Valtchev, J. Patarin, A. C. Faust and B. Maquin, *Microporous and Mesoporous Materials*, 2002, **56**, 175-184.
14. V. Valtchev, B. J. Schoeman, J. Hedlund, S. Mintova and J. Sterte, *Zeolites*, 1996, **17**, 408-415.
15. V. Valtchev, J. Hedlund, B. J. Schoeman, J. Sterte and S. Mintova, *Microporous Materials*, 1997, **8**, 93-101.
16. R. J. Tayade, R. G. Kulkarni and R. V. Jasra, *Industrial & engineering chemistry research*, 2007, **46**, 369-376.
17. S. Sampath, H. Uchida and H. Yoneyama, *Journal of Catalysis*, 1994, **149**, 189-194.
18. K. Kočí, L. Obalová and Z. Lacný, *Chemical Papers*, 2008, **62**, 1-9.
19. R. J. Tayade, R. G. Kulkarni and R. V. Jasra, *Industrial & Engineering Chemistry Research*, 2006, **46**, 369-376.
20. Y. Xu and C. H. Langford, *The Journal of Physical Chemistry B*, 1997, **101**, 3115-3121.
21. H. Ichiura, T. Kitaoka and H. Tanaka, *Journal of materials science*, 2002, **37**, 2937-2941.
22. S. Fukahori, H. Ichiura, T. Kitaoka and H. Tanaka, *Environmental science & technology*, 2003, **37**, 1048-1051.
23. S. Kumar, T. M. Davis, H. Ramanan, R. L. Penn and M. Tsapatsis, *The Journal of Physical Chemistry B*, 2007, **111**, 3398-3403.
24. A. J. Maira, W. N. Lau, C. Y. Lee, P. L. Yue, C. K. Chan and K. L. Yeung, *Chemical Engineering Science*, 2003, **58**, 959-962.
25. A. Kafizas, S. Kellici, J. A. Darr and I. P. Parkin, *Journal of Photochemistry and Photobiology a-Chemistry*, 2009, **204**, 183-190.
26. K. Page, R. G. Palgrave, I. P. Parkin, M. Wilson, S. L. P. Savin and A. V. Chadwick, *Journal of Materials Chemistry*, 2007, **17**, 95-104.
27. A. Rampaul, I. P. Parkin, S. A. O'Neill, J. DeSouza, A. Mills and N. Elliott, *Polyhedron*, 2003, **22**, 35-44.
28. I. Georgiadou, N. Spanos, C. Papadopoulou, H. Matralis, C. Kordulis and A. Lycourghiotis, *Colloids and Surfaces a-Physicochemical and Engineering Aspects*, 1995, **98**, 155-165.
29. S. Arab, D. Li, N. Kinsinger, F. Zaera and D. Kisailus, *Journal of Materials Research*, 2011, **26**, 2653-2659.
30. J. L. Ong, L. C. Lucas, G. N. Raikar and J. C. Gregory, *Applied Surface Science*, 1993, **72**, 7-13.
31. T. Gross, M. Ramm, H. Sonntag, W. Unger, H. M. Weijers and E. H. Adem, *Surface and Interface Analysis*, 1992, **18**, 59-64.
32. M. L. Miller and R. W. Linton, *Analytical Chemistry*, 1985, **57**, 2314-2319.
33. W. E. Slink and P. B. DeGroot, *Journal of Catalysis*, 1981, **68**, 423-432.
34. T. Ohsaka, F. Izumi and Y. Fujiki, *Journal of Raman Spectroscopy*, 1978, **7**, 321-324.
35. J. Qi, T. B. Zhao, X. Xu, F. Y. Li and G. D. Sun, *J Porous Mater*, 2011, **18**, 509-515.
36. M. K. Naskar, D. Kundu and M. Chatterjee, *Bulletin of Materials Science*, 2009, **32**, 537-541.
37. S. Kundu, A. Kafizas, G. Hyett, A. Mills, J. A. Darr and I. P. Parkin, *Journal of Materials Chemistry*, 2011, **21**, 6854-6863.
38. A. Mills, J. Wang, S.-K. Lee and M. Simonsen, *Chemical communications*, 2005, 2721-2723.
39. A. Mills and J. Wang, *Journal of Photochemistry and Photobiology A: Chemistry*, 2006, **182**, 181-186.
40. H. Hantsche, *Advanced Materials*, 1993, **5**, 778-778.

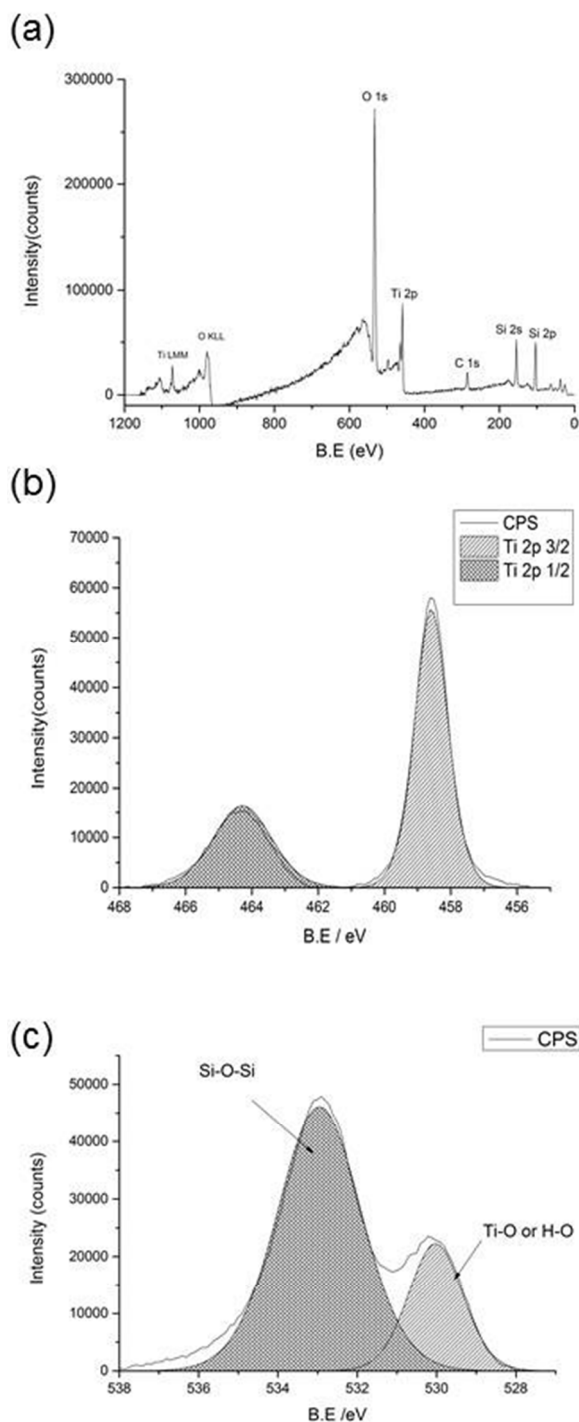


Figure 2 – X-ray photoelectron spectroscopy survey spectra of a typical TiO<sub>2</sub>/Si/glass fibre material. The XPS high resolution spectra consist of characteristic Ti 2p<sub>3/2</sub> and 2p<sub>1/2</sub> doublet and O 1s peaks.

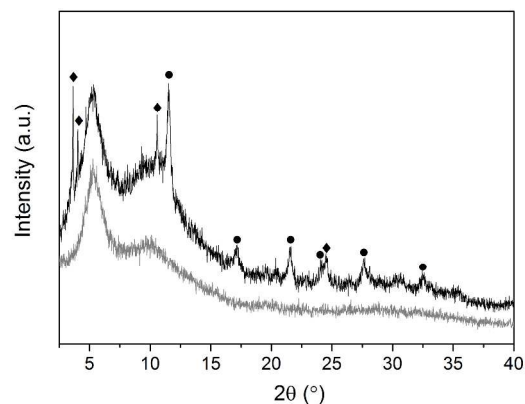


Figure 3 – X-ray diffraction patterns of a typical TiO<sub>2</sub>/Si/glass fibre material (black line). The peaks from both anatase TiO<sub>2</sub> (full circles) and silicalite-1 zeolite (full diamonds) are indicated. The diffraction signal from the glass substrate is included for reference (grey line).

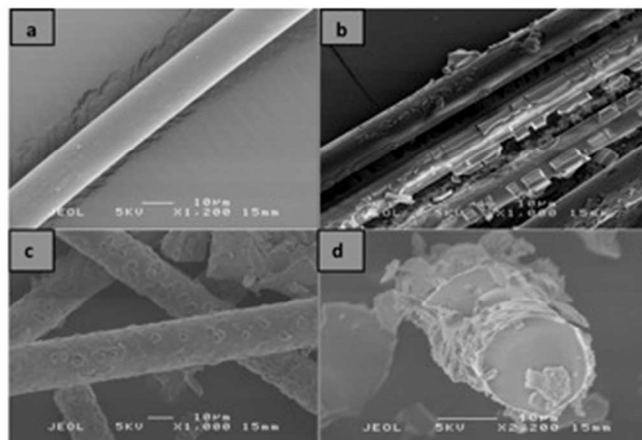


Figure 4 – Scanning electron microscopy images of (a) glass fibre, (b) TiO<sub>2</sub> coating on plain glass fibre, (c) and (d) Silicalite-1 coating on glass fibre (samples 2A and 3B, respectively).

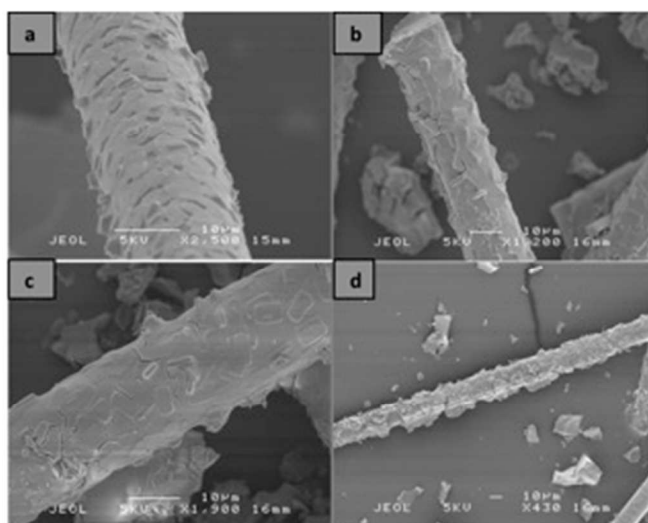


Figure 5 – Scanning electron microscopy images of a range of TiO<sub>2</sub>/silicalite-1/fibre samples: (a) sample 2A, (b) sample 4A and (c) and (d) sample 4B.

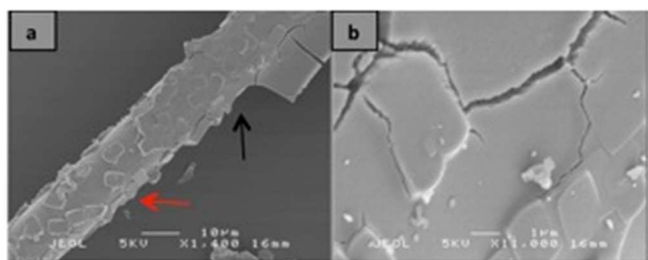


Figure 6 – Scanning electron microscopy images highlighting (a) the different aspects of the TiO<sub>2</sub> coating (black arrow) and the silicalite-1 coating (red arrow) and (b) cracks on the TiO<sub>2</sub> coating as a result of the annealing procedure.

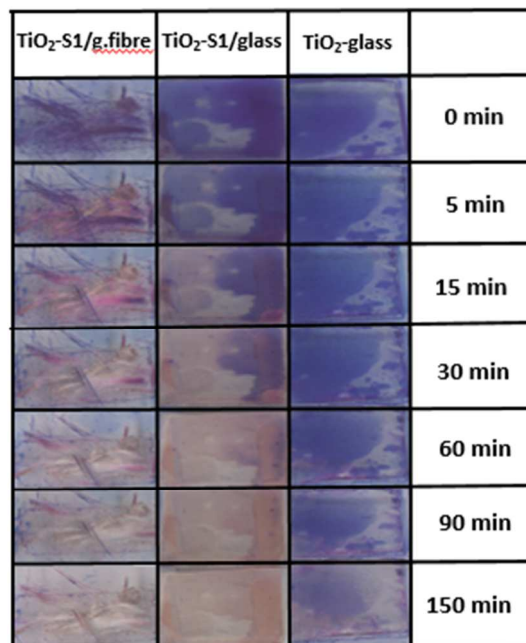


Figure 7 – Selected photographs taken during the resazurin ink test on TiO<sub>2</sub>/S1/fibre, TiO<sub>2</sub>/S1/glass slide and TiO<sub>2</sub>/glass slide materials under UVA irradiation (1 mW cm<sup>-2</sup>) over 150 min.

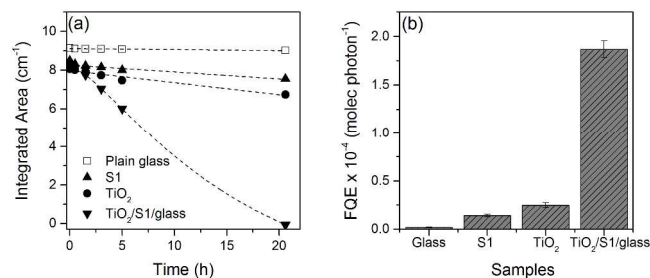


Figure 8 – (a) Curves of integrated areas of stearic acid IR bands and (b) corresponding photocatalytic activities, given formal quantum efficiencies, during UVA irradiation (3.7 mW cm<sup>-2</sup>) of a TiO<sub>2</sub>/S1/glass sample and respective individual components, as indicated. The corresponding areas of acid on plain glass (no photocatalyst) are included for reference (empty symbols).